

Probing the Topological Phase Transition via Density Oscillations in Silicene and Germanene

Hao-Ran Chang,¹ Jianhui Zhou,^{2,*} Hui Zhang,³ and Yugui Yao⁴

¹*Department of Physics and Institute of Solid State Physics,
Sichuan Normal University, Chengdu, Sichuan 610066, China*

²*Department of Physics, Carnegie Mellon University, Pittsburgh, Pennsylvania 15213, USA*

³*Department of Physics and Astronomy, Ohio University, Athens, Ohio 45701, USA*

⁴*School of Physics, Beijing Institute of Technology, Beijing 100081, China*

We theoretically investigated two kinds of density oscillations, the Friedel oscillation and collective excitation in the silicene and germanene within the random phase approximation, and found that the tunable spin-valley coupled band structure could lead to some exotic properties in these two phenomena. Based on an exact analytical and numerical analysis, we demonstrated that the beating of the screened potential as well as the undamped plasmon mode can be taken as fingerprints of a topological phase transition in doped silicene and doped germanene. Thus our proposal here establishes the connection between the topological phase transition and the density oscillations that can be accessed by a variety of experimental techniques.

PACS numbers: 73.43.-f, 73.22.Lp, 71.45.Gm

The quantum spin Hall effect (QSHE) [1, 2] has been studied extensively in both theoretical and experimental aspects. It is well known that topologically protected helical edge states are a distinct feature which characterizes the QSHE [3]. The transport measurement of edge states requires that the bulk state must be insulating. In practice, the system is usually metallic resulting from defects, self-doping and charge transfer from metallic substrates, and thus the detection of the topological phase transition (TPT) when the bulk is metallic becomes urgent and important in two-dimensional systems. In this Rapid Communication, we connect the TPT with two kinds of density oscillations: Friedel oscillation [4] and collective excitation in silicene and germanene.

Silicene [5, 6], a single layer of silicon atoms forming a two-dimensional (2D) buckled honeycomb lattice, can be regarded as the silicon-based counterpart of graphene [7]. The buckled honeycomb structure gives rise to a tunable spin-valley coupled band structure, which accounts for many exotic transport and superconducting phenomena [8–14] and makes silicene a promising candidate for the QSHE [15]. So far silicene or its superstructure has only been synthesized on metallic surfaces [16–19], hence the transport measurement of the helical edge states is prevented due to the metallic bulk state. On the other hand, it has been claimed that a Dirac-like spectrum does exist in silicene from experimental observations [16, 17]. Although there is some debate about the origin of the linear dispersion [20], it is still highly worthwhile to examine whether or not silicene hosts the QSH state.

In this Rapid Communication, we propose a detection method of TPT by employing both the Friedel oscillation and collective excitation in silicene, and show how to extract the information about the TPT from these two

effects. First, the screened potential of charged impurities has a beating structure of Friedel oscillations (the interference pattern of two branches of density waves of electrons). As one band gap decreases (for example, the spin-up gap in Fig. 1), the beating of the screened potential gradually becomes faint and eventually vanishes at the TPT point. Second, the undamped plasmon mode (UPM) that emerges in the single-particle excitation (SPE) gap disappears when approaching the TPT point and reappears after it. Therefore, these two kinds of density oscillations can be used to detect the TPT in metallic silicene and germanene.

We start from a simple low-energy effective Hamiltonian in silicene under an external electric field [15, 21],

$$\hat{H}_\xi = \hbar v_F (\xi k_x \tau_x + k_y \tau_y) - \xi \Delta_{so} \sigma_z \tau_z / 2 + \Delta_z \tau_z / 2, \quad (1)$$

where the subscripts $\xi = \pm$ denote the two inequivalent valleys or Dirac points K_+ and K_- , respectively. The first term describes the behavior of 2D Dirac electrons with the Fermi velocity v_F . The second term is the intrinsic spin orbit coupling (SOC) term with a magnitude of Δ_{so} . The last term is due to the $A - B$ sublattice symmetry breaking and is defined as $\Delta_z = E_z \cdot d$, where E_z is the effective external electric field perpendicular to the sample including all of the screening effect, and d is the perpendicular distance between the two sublattice planes. Pauli matrices τ_i and σ_i act on the pseudospin space related to the A and B sublattices and the real spin degree of freedom, respectively. Since the strength of the intrinsic Rashba SOC is much smaller than that of the intrinsic SOC [21], we can neglect it here. Thus, the effective Hamiltonian can be classified by the eigenvalues of σ_z and the corresponding Hamiltonian of the K_+ valley can be expressed as

$$\hat{h}_\sigma = \begin{pmatrix} (\Delta_z - \sigma \Delta_{so}) / 2 & \hbar v_F (k_x - i k_y) \\ \hbar v_F (k_x + i k_y) & -(\Delta_z - \sigma \Delta_{so}) / 2 \end{pmatrix}, \quad (2)$$

*Electronic address: jhzhou@andrew.cmu.edu

where $\sigma = \pm$ refer to the spin-up and spin-down bands, respectively. Two remarks are in order. First, the corresponding Hamiltonian of the K_- valley can be obtained from Eq.(2) via the time reversal operation. Second, we assume that there are no short-range impurities and defects that cause intervalley scattering. Accordingly, we are able to restrict our discussion to the case of a single valley, and then multiply the valley-degeneracy factor $g_v = 2$ to the final results. The eigenvalues of the effective Hamiltonian in Eq.(2) can be evaluated straightforwardly as $E_{\sigma\lambda} = \lambda\sqrt{\hbar^2 v_F^2 k^2 + \Delta_\sigma^2}$, where $\lambda = \pm$ are for the conduction and valence bands, and $2\Delta_\pm = \Delta_{so} |\gamma \mp 1|$ are the spin dependent energy gaps with $\gamma = \Delta_z / \Delta_{so}$.

Before presenting the detailed calculations, we first discuss the topological phases of our model Hamiltonian. The model would describe the gapless graphene for $\Delta_{so} = 0$ and gapped graphene for $\Delta_{so} \neq 0$ and $\gamma = 0$, [see Fig. 1(a)]. When $\Delta_{so} \neq 0$ and $\gamma \neq 0$, the model will account for silicene. The region for $|\gamma| < 1$ pertains to the QSH state with a pair of helical edge states, as shown in Fig. 1(b), and for $|\gamma| > 1$ the system is the usual band insulator without any topological edge states [see Fig. 1(d)]. Interestingly, when $\gamma = 1$, i.e., $\Delta_z = \Delta_{so}$, at the K_+ valley the spin-up band becomes gapless and the gap of the spin-down band is Δ_{so} , as shown in Fig. 1(c), while at the K_- valley the spin reverses, which has been termed a valley-spin-polarized semimetal [8] and is a unique characteristic of silicene.

In the following we want to investigate the Friedel oscillation and the plasmon spectrum. The analytic dielectric function within the random phase approximation (RPA) is given by

$$\varepsilon(q, \omega) = 1 - V(q)\chi_0(q, \omega), \quad (3)$$

where $V(q) = 2\pi e^2 / \kappa q$ is the Fourier transform of the 2D Coulomb interaction, $V(r) = e^2 / \kappa r$, and κ is the effective background dielectric constant [22]. The full formal expression of the polarization function in silicene is given by [23]

$$\chi_0(q, \omega) = g_v \sum_{\lambda, \lambda', \sigma = \pm} \int \frac{d^2 k}{(2\pi)^2} |\langle \psi_{\sigma\lambda}(\mathbf{k}) | \psi_{\sigma\lambda'}(\mathbf{k}') \rangle|^2 \times \frac{n_F[E_{\sigma\lambda}(\mathbf{k})] - n_F[E_{\sigma\lambda'}(\mathbf{k}')] }{\hbar\omega + E_{\sigma\lambda}(\mathbf{k}) - E_{\sigma\lambda'}(\mathbf{k}') + i\eta}, \quad (4)$$

where $|\psi_{\sigma\lambda}(\mathbf{k})\rangle$ is the eigenstate corresponding to $E_{\sigma\lambda}$, η is a positive infinitesimal quantity, $\mathbf{k}' = \mathbf{k} + \mathbf{q}$, and $n_F(x) = [\exp\{\beta(x - \mu)\} + 1]^{-1}$, with $\beta = 1/k_B T$. Noted that since the spin-up component and spin-down component decouple with each other, the total polarization function turns out to be the summation of those for both spin species. The polarization function for a certain spin species in silicene is mathematically identical to the case of a gapped graphene.

To proceed with the theoretical details, we assume zero temperature $T = 0$ K, and then the noninteracting Fermi function $n_F(x)$ turns into a simple step function $\theta(\mu - x)$.

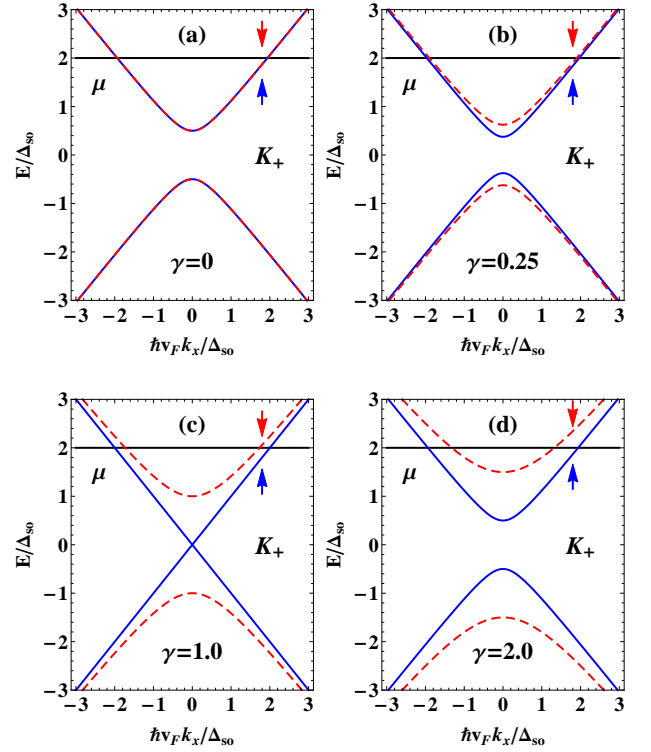


FIG. 1: (Color online) The band structures at the K_+ valley for different γ 's. The solid blue line represents the spin-up band while the dashed red line corresponds to the spin-down band.

We restrict our discussion to positive frequencies $\omega > 0$ because of the general relation $\chi_0(q, -\omega) = [\chi_0(q, \omega)]^*$. Due to the electron-hole symmetry, the plasmon in both n - and p -doped samples would show the same dynamical behaviors. Therefore, we can concentrate on the n -doped case, namely, the finite chemical potential μ lies in the conduction band. Since when $\Delta_+ \leq \mu \leq \Delta_-$ there is no beating in the screened potential, in our discussion of Friedel oscillation, we require that the Fermi contour consists of two Fermi circles with different Fermi wave vectors, $k_F^\sigma = \sqrt{\mu^2 - \Delta_\sigma^2} / \hbar v_F$ as long as the external electric field changes.

The static screened potential of a charged impurity is given by the integration of the dielectric function,

$$\phi(r) = \frac{Ze}{\kappa} \int_0^\infty dq \frac{J_0(qr)}{\varepsilon(q, 0)}, \quad (5)$$

where $\varepsilon(q, 0) = 1 - V(q)\chi_0(q, 0)$ is the static dielectric function, Ze the charge of the impurity and $J_0(x)$ the zeroth order Bessel function of the first kind, which comes from the integration over the angular variable. After some cumbersome manipulations, one can obtain the static wave vector dependent polarization function from Eq.(4),

$$\chi_0(q, 0) = -\frac{2\mu}{\pi \hbar^2 v_F^2} \left[1 - \sum_{\sigma = \pm} \theta(q - 2k_F^\sigma) \left(\frac{\sqrt{q^2 - 4k_F^\sigma{}^2}}{4q} \right) \right]$$

$$-\frac{\hbar^2 v_F^2 q^2 - 4\Delta_\sigma^2}{8\hbar v_F q \mu} \arctan \frac{\hbar v_F \sqrt{q^2 - 4k_F^{\sigma 2}}}{2\mu} \Big). \quad (6)$$

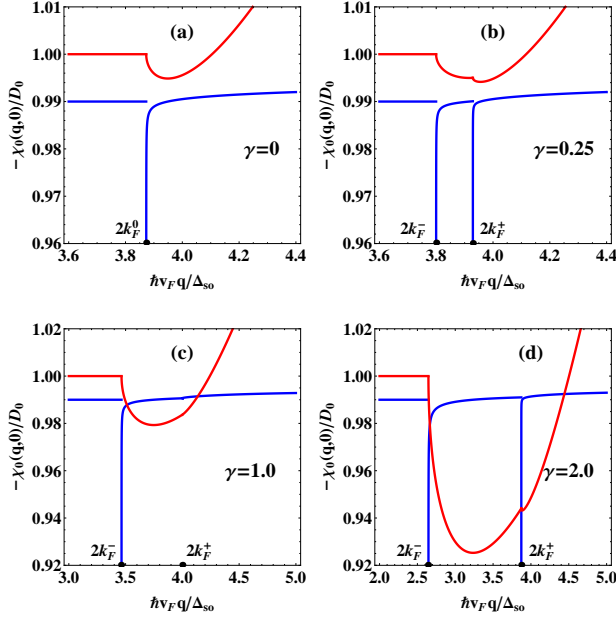


FIG. 2: (Color online) Static real part of the charge susceptibility (red line) in units of the density of states $D_0 = 2\mu/\pi\hbar^2 v_F^2$, and its corresponding first derivative is schematically represented by the blue line.

Therefore, the screened potential can be obtained from Eq.(5) by numerical integration over q (see Fig. 3). At a large distance from the charged impurity ($k_F^- r \gg 1$), there are two main contributions to the screened potential. The first part is the Thomas-Fermi contribution, $\phi(r) = Ze\hbar^2 v_F^2 / 16\kappa\alpha_\kappa^2 \mu^2 r^3$ with $\alpha_\kappa = e^2 / \kappa\hbar v_F$ the effective fine structure constant, which is determined by the long-wavelength ($q \rightarrow 0$) behavior of the polarization function, $\chi_0(q < 2k_F^-, 0) = -2\mu/\pi\hbar^2 v_F^2$. The scale $1/r^3$ of the screened potential at the long-wavelength limit can also be found in the traditional 2D electron gas (2DEG) [24], gapless and gapped graphene [25–30].

The second part is oscillatory, the Friedel oscillation [4]. The Lighthill theorem [5] states that singularities in the derivatives of the polarization function lead to an algebraic, and oscillating decay of the screened potential. For the case $\gamma \neq 1$ ($\Delta_\pm \neq 0$), the first derivative of the polarization function is discontinuous at $q = 2k_F^\pm$. For the case $\gamma = 1$ ($\Delta_+ = 0$ and $\Delta_- \neq 0$), the first derivative of the polarization function is discontinuous at $q = 2k_F^-$ but continuous at $q = 2k_F^+$, and the second derivative of the polarization function is singular at $q = 2k_F^+$. Thus, the asymptotic screened potential is a superposition of two kinds of oscillations, which gives rise to a *beating* in the oscillatory part of the screened potential as (see the Supplemental Material [32]),

$$\phi_{\gamma \neq 1}(r) \approx \frac{Ze}{\kappa} [F_-(r) + F_+(r)], \quad (7)$$

$$\phi_{\gamma=1}(r) \approx \frac{Ze}{\kappa} [F_-(r) + G_+(r)], \quad (8)$$

where the functions $F_\pm(r)$, $G_+(r)$, and f_\pm are given by

$$F_\pm(r) = -\frac{\alpha_\kappa \hbar v_F \Delta_\pm^2}{2\mu(\hbar v_F k_F^\pm + 2\alpha_\kappa \mu f_\pm)^2} \frac{\sin(2k_F^\pm r)}{r^2}, \quad (9)$$

$$G_+(r) = \frac{\alpha_\kappa \hbar^2 v_F^2}{4\mu^2(1 + 2\alpha_\kappa f_+)^2} \frac{\cos(2k_F^+ r)}{r^3}, \quad (10)$$

$$f_\pm = 1 - \frac{1 \pm 1}{2} \left(\frac{\sqrt{k_F^{+2} - k_F^{-2}}}{4k_F^+} \right) - \frac{\hbar^2 v_F^2 k_F^{+2} - \Delta_-^2}{4\hbar v_F k_F^+ \mu} \arctan \frac{\hbar v_F \sqrt{k_F^{+2} - k_F^{-2}}}{\mu}. \quad (11)$$

It should be noted that the discrepancy between the oscillatory decay $\sin(2k_F r)/r^2$ in gapped graphene [29, 30] and $\cos(2k_F r)/r^3$ in gapless graphene [25] is because of the unique π Berry phase of each Dirac point in gapless graphene that suppresses the backscattering of particles on the Fermi surface during intravalley scattering [33].

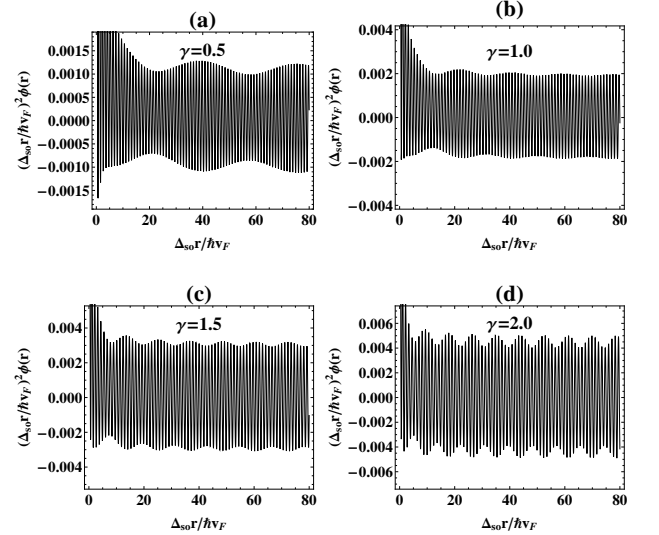


FIG. 3: The beating behavior of the screened potential (in units of $Ze\Delta_{so}/\kappa\hbar v_F$) vs the ratios γ for $\kappa = 3$, $\mu = 3\Delta_{so}$, and $v_F = c/550$.

When $\gamma \neq 0, 1$, both the spin-up and spin-down bands are gapped, and therefore the static polarizability has two cusps and its first derivative is singular at $q = 2k_F^\pm$ [see Figs. 2(b) and 2(d)]. The corresponding oscillatory potential is displayed in Figs. 3(a, 3(c), and 3(d). For a gapped graphene with $\gamma = 0$, the two Fermi wave vectors k_F^σ become degenerate so that only one cusp of static polarizability remains, and the singularity of its first derivative locates at $q = 2k_F^0$ (with $k_F^+ = k_F^- \equiv k_F^0$) [see Fig. 2(a)]. Therefore there is only a one-component Friedel oscillation which does not support beating. Interestingly, at the TPT point $\gamma = 1.0$, the polarization

function has a cusp at $q = 2k_F^-$, and its first derivative is continuous at $q = 2k_F^+$ but discontinuous at $q = 2k_F^-$, as shown in Fig. 2(c). Thus the screened potential turns out to be a superposition of $\cos(2k_F^+ r)/r^3$ for gapless graphene with $k_F^+ = \mu/\hbar v_F$ and $\sin(2k_F^- r)/r^2$ for gapped graphene with $k_F^- = \sqrt{\mu^2 - \Delta_{so}^2}/\hbar v_F$. Since the latter overwhelmingly dominates in magnitude at a large distance, the superposition of these two oscillating parts does not have an indistinguishable beating as shown in Fig. 3(b). Note that the screened potentials can be captured by our approximative expressions in Eqs.(7) and (8) (more details can be found in the Supplemental Material [32]).

From Figs. 3(a)-3(d), one can clearly see that as the ratio γ approaches 1, the beating gets gradually faint and disappears at the TPT point. Once crossing the TPT point, the beating of the oscillatory potential becomes noticeable. Therefore, the evolution of the beating can be seen as a fingerprint of TPT in metallic silicene. Note that the beating in the topological phase is usually much longer than the counterpart in the normal phase, which provides us with quantitative evidence of the topological nature of the phase. The Friedel oscillation can be extracted from the differential tunneling conductance using scanning tunneling spectroscopy (STS), which has been used to investigate the Friedel oscillation in a $\sqrt{3} \times \sqrt{3}$ superstructure of silicene on Ag(111) [35]. Therefore, we expect that further STS measurements on the Friedel oscillation of silicene could be used to identify the TPT tuned by the external electrical fields.

We now turn to calculate the plasmon dispersion $\omega_p(q)$ by solving the following equation,

$$\varepsilon(q, \omega_p - i\delta) = 0, \quad (12)$$

where δ is the decay rate of the plasmons. At small energies and momenta $\hbar v_F q \ll \hbar\omega \ll \mu$ with $\Delta_+ \leq \Delta_- < \mu$, one can obtain the polarization function in the long-wavelength limit,

$$\chi_0(q, \omega) \approx \mu q^2 [2 - (\Delta_+^2 + \Delta_-^2)/\mu^2] / (2\pi\hbar^2\omega^2). \quad (13)$$

Hence, one immediately obtains the corresponding plasmon frequencies,

$$\omega_p^0(q) \approx \sqrt{\alpha_\kappa \mu v_F [2 - (\Delta_+^2 + \Delta_-^2)/\mu^2] q / \hbar}. \quad (14)$$

We note that $\omega_p^0(q) \propto \sqrt{q}$ is a peculiarity of 2D plasmon dispersions including both the 2DEG and Dirac fermions. In Figs. 4(a)-4(c), we show the exact numerical plasmon dispersion within RPA (solid red line) and the long-wavelength plasmon (LWP) (dashed blue line). The SPE region is given by $\text{Im}[\chi_0(q, \omega)] \neq 0$ and displayed as shaded areas in the (q, ω) space, where the plasmon is damped into electron-hole pairs (Landau damping). As shown in Figs. 4(a)-4(c), the LWP frequency ω_p^0 is well consistent with the exact numerical solution ω_p in the small wave vector regime.

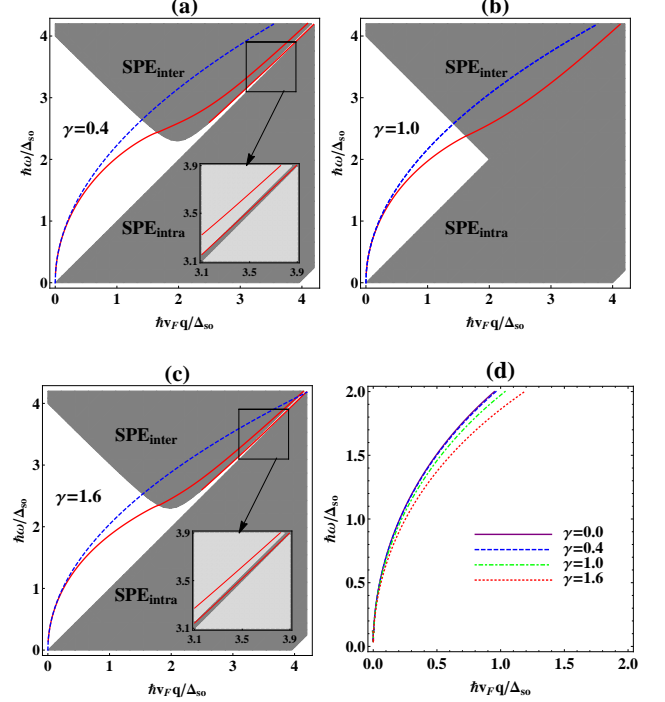


FIG. 4: (Color online) The numerical exact solution within RPA (red) and the long-wavelength plasmon frequency (blue), with the shaded areas representing the interband and the intraband SPE regions. (d) shows the effect of γ on the plasmon frequency. In the inset of (a) or (c), there is a clear UPM in the SPE gap [34].

At the TPT point ($\gamma = 1$), there exists only one plasmon mode which is undamped until it enters the interband SPE region. Note that this branch of the plasmon had been studied extensively in the context of graphene and a number of exciting applications were proposed for plasmonics [36]. Apart from the TPT point, the exact numerical solution displays two plasmon modes: One branch of the plasmon is mentioned above, and the other is a UPM that emerges in the SPE gap [see the insets of Figs. 4(a)-4(c)]. This UPM can be observed by infrared optical spectroscopy [37], angular-resolved photoemission spectroscopy [38], and other methods [36]. It should be noted that although our UPM has been found in gapped graphene, the observation in practice is still hard to achieve because of the weak interaction with the substrate or the small intrinsic SOC. To protect the UPM against the thermal effects and impurity scattering requires a large SPE gap, which is mainly determined by the SOC gap. The SOC gaps are about 1.55 and 24.0 meV for silicene and germanene, respectively [15]. For silicene, its corresponding energy ranges from 1 to 10 meV by tuning the chemical potential and it can be detected experimentally on insulating substrates. For germanene, the energy of UPM is an order of magnitude larger than that of silicene and is accessed by some experimental methods on both insulating and metallic

substrates [39].

Compared with gapped graphene [28–30], the tunable spin-valley coupled band structure in silicene gives rise to two additional features in the plasmon spectrum. First, as shown in Fig. 4(d), the plasmon frequencies have red-shifted as the ratio γ increases by adjusting the electric field, which can be read out from the long-wavelength solution in Eq.(14). Second, the UPM in the SPE gap decays into a SPE continuum at the TPT point and then reappears after the system separates from the TPT point. When closing to the TPT point ($\gamma \rightarrow 1$), the system has a very tiny band gap, and the thermal fluctuation or disorder scattering could smear the small gap and eventually destroy the UPM. Hence, the disappearance of the UPM can take place in a small region around $\gamma = 1$ in the spectral function and help us to identify the TPT point. Therefore, the fate of the UPM indeed reflects the change of the topology of energy bands. Furthermore, combining with LWP, the behavior of the plasmons can clearly characterize the topological nature of the phase. For instance, when the system is in the normal phase with $1 < \gamma$, decreasing the electric field E_z makes the LWP have a violetshift and the UPM disappears near the TPT point and then reappears in the topological phase. Discussions of other situations are similar.

In summary, we explored Friedel oscillations and collective excitation in silicene and germanene within RPA. We emphasize that the tunable spin-valley coupled band structure could cause some exotic properties in these two phenomena. We demonstrate that the beating of the screened impurity potential and the behavior of UPM can both be used as probes for TPT in silicene and germanene. Our work sheds light on the identification of TPT via some physical effects. The distinct features of the density oscillations can also provide us with some hints on how to resolve controversy concerning the origin of the linear dispersion.

Note added. Recently, we became aware of a similar work in this field [40].

We are grateful to G. Z. Liu, P. K. Pyatkovskiy, K. H. Wu, D. Xiao, F. Zhang and F. R. Zhang for favorable discussions and comments. This work is supported in part by the MOST Project of China under Grant No. 2014CB920903, the Scientific Research Fund of the Education Department of Sichuan Province under Grant No. 13ZB0157, the NSFC under Grants No. 11074234, No.11274286, No.11174337 and No.11225418, and the U.S. Department of Energy, Office of Basic Energy Sciences, Materials Sciences and Engineering Division.

-
- [1] C. L. Kane and E. J. Mele, Phys. Rev. Lett. **95**, 226801 (2005).
 - [2] B. A. Bernevig, T. L. Hughes, and S. C. Zhang, Science, **314**, 1757 (2006).
 - [3] M. König, S. Wiedmann, C. Brüne, A. Roth, H. Buhmann, L. W. Molenkamp, X.-L. Qi, and S.-C. Zhang, Science, **318**, 766 (2007).
 - [4] J. Friedel, Nuovo Cimento Suppl. **7**, 287 (1958).
 - [5] G. G. Guzman-Verri and L. C. Lew Yan Voon, Phys. Rev. B **76**, 075131 (2007).
 - [6] S. Cahangirov, M. Topsakal, E. Aktürk, H. Şahin, and S. Ciraci, Phys. Rev. Lett. **102**, 236804 (2009).
 - [7] Because of the similarity between the germanene and the silicene, for the remainder of this Rapid Communication, we will not mention the germanene unless it is necessary.
 - [8] M. Ezawa, Phys. Rev. Lett. **109**, 055502 (2012).
 - [9] W. F. Tsai, C. Y. Huang, T. R. Chang, H. Lin, H. T. Jeng, and A. Bansil, Nat. Commun. **4**:1500 (2013).
 - [10] H. Z. Lu, W. Yao, D. Xiao, and S. Q. Shen, Phys. Rev. Lett. **110**, 016806 (2013).
 - [11] H. Pan, Z. Li, C.-C. Liu, G. Zhu, Z. Qiao, and Y. Yao, Phys. Rev. Lett. **112**, 106802 (2014).
 - [12] F. Liu, C.-C. Liu, K. Wu, F. Yang, and Y. Yao, Phys. Rev. Lett. **111**, 066804 (2013).
 - [13] W. Wan, Y. Ge, F. Yang and Y. Yao, EPL **104**, 36001 (2013).
 - [14] L. Zhang, F. Yang, Y. Yao, arXiv:1309.7347.
 - [15] C.-C. Liu, W. X. Feng, and Y. G. Yao, Phys. Rev. Lett. **107**, 076802 (2011).
 - [16] L. Chen, C.-C. Liu, B. Feng, X. He, P. Cheng, Z. Ding, S. Meng, Y. Yao, and K. Wu, Phys. Rev. Lett. **109**, 056804 (2012).
 - [17] P. Vogt, P. De Padova, C. Quaresima, J. Avila, E. Frantzeskakis, M. C. Asensio, A. Resta, B. Ealet, and G. Le Lay, Phys. Rev. Lett. **108**, 155501 (2012).
 - [18] A. Fleurence, R. Friedlein, T. Ozaki, H. Kawai, Y. Wang and Y. Yamada-Takamura, Phys. Rev. Lett. **108**, 245501 (2012).
 - [19] L. Meng, Y. Wang, L. Zhang, S. Du, R. Wu, L. Li, Y. Zhang, G. Li, H. Zhou, W. A. Hofer, and H.-J. Gao, Nano Lett. **13**, 685 (2013).
 - [20] Y. P. Wang and H. P. Cheng, Phys. Rev. B **87**, 245430 (2013).
 - [21] C. C. Liu, H. Jiang, and Y. G. Yao, Phys. Rev. B **84**, 195430 (2011).
 - [22] The effective dielectric constant $\kappa = (\kappa_a + \kappa_b)/2$ is the average screening contribution of any dielectrics above (κ_a) and below (κ_b) the sample. The different values of κ do not modify the qualitative behavior.
 - [23] K. W.-K. Shung, Phys. Rev. B. **34**, 979 (1986).
 - [24] F. Stern, Phys. Rev. Lett. **18**, 546 (1967).
 - [25] B. Wunsch, T. Stauber, F. Sols and F. Guinea, New Journal of Physics, **8**, 318 (2006).
 - [26] E. H. Hwang and S. Das Sarma, Phys. Rev. B **75**, 205418 (2007).
 - [27] M. Polini, R. Asgari, G. Borghi, Y. Barlas, T. Pereg-Barnea, and A. H. MacDonald, Phys. Rev. B **77**, 081411 (2008).
 - [28] X. F. Wang and T. Chakraborty, Phys. Rev. B **75**, 033408 (2007).
 - [29] P. K. Pyatkovskiy, J. Phys.: Condens. Matter **21**, 025506 (2009).
 - [30] A. Scholz, T. Stauber and J. Schliemann, Phys. Rev. B **86**, 195424 (2012).

- [31] M. J. Lighthill, *Introduction to Fourier Analysis and Generalized Functions* (Cambridge University Press, Cambridge, U.K., 1958).
- [32] See Supplemental Material for a detailed derivation of the oscillatory part of the screened potential.
- [33] T. Ando, T. Nakanishi and R. Saito, J. Phys. Soc. Jpn. **67**, 2857 (1998).
- [34] In our numerical calculation, we take $\kappa = 3$, $\mu = 2\Delta_{so}$, and $v_F = c/550$.
- [35] B. Feng, H. Li, C.-C. Liu, T.-N. Shao, P. Cheng, Y. Yao, S. Meng, L. Chen, and K. Wu, ACS Nano, **7**, 9049 (2013).
- [36] A. N. Grigorenko, M. Polini, and K. S. Novoselov, Nature Photonics **6**, 749 (2012).
- [37] Z. Fei, G. O. Andreev, W. Bao, L. M. Zhang, A. S. McLeod, C. Wang, M. K. Stewart, Z. Zhao, G. Dominguez, M. Thiemens, M. M. Fogler, M. J. Tauber, A. H. Castro-Neto, C. N. Lau, F. Keilmann, and D. N. Basov, Nano Lett. **11**, 4701 (2011).
- [38] A. Bostwick, F. Speck, T. Seyller, K. Hom, M. Polini, R. Asgari, A. H. MacDonald, E. Rotenberg, Science, **328**, 999 (2010).
- [39] In our simulations, the UPM's frequency is in the order of 10-100 meV, and within this region, one simple calculation within classical electromagnetic theory gives the same order amplitude in the absorption resonance of germanene compared with the background spectra of the Ag substrate. Also, when the absorption peak occurs at larger than 50 meV, the plasmon resonance would not be damped by the Ag substrate due to the small relaxation time of Ag (50 fs corresponds to 12 meV). Furthermore, usually the energies of the surface and bulk plasmon resonances of the metallic substrate lie in the order 1 eV (Ag is 3 eV while Au is 2.2 eV), and they are far away from that of germanene, with the result that the interference between the plasmon resonances of the substrate and germanene is nearly impossible. All three factors make the plasmon resonances of germanene observable in experiments, even in an Ag substrate.
- [40] C. J. Tabert and E. J. Nicol, Phys. Rev. B **89**, 195410 (2014).

Supplementary material for “Probing the Topological Phase Transition via Density Oscillations in Silicene and Germanene”

I. PRELIMINARY

In this supplementary material we present the major steps of calculating the screened potential of silicene at large distance by following the method [1]. As indicated in the main text, the screened potential takes the form

$$\phi(r) = \frac{Ze}{\kappa} \int_0^\infty \frac{J_0(qr)}{\varepsilon(q, 0)} dq, \quad (\text{S.1})$$

where the static dielectric function $\varepsilon(q, 0) = 1 - V(q)\chi_0(q, 0)$ with $V(q) = 2\pi e^2/\kappa q$. When the Fermi level cuts two Fermi surfaces ($\Delta_+ \leq \Delta_- < \mu$), according to Eq.(6) in the main text the static dielectric function is of the form

$$\varepsilon(q, 0) = 1 + \frac{4\alpha_\kappa\mu}{\hbar v_F q} \left[1 - \sum_{\sigma=\pm} \theta(q - 2k_F^\sigma) \left(\frac{\sqrt{q^2 - 4k_F^{\sigma 2}}}{4q} - \frac{\hbar^2 v_F^2 q^2 - 4\Delta_\sigma^2}{8\hbar v_F q \mu} \arctan \frac{\hbar v_F \sqrt{q^2 - 4k_F^{\sigma 2}}}{2\mu} \right) \right]. \quad (\text{S.2})$$

For the sake of simplicity, we introduce some dimensionless quantities,

$$\tilde{q} = \frac{\hbar v_F q}{\Delta_{so}}, \quad \tilde{r} = \frac{\Delta_{so} r}{\hbar v_F}, \quad \tilde{\mu} = \frac{\mu}{\Delta_{so}}, \quad \tilde{\Delta}_\sigma = \frac{\Delta_\sigma}{\Delta_{so}}, \quad \tilde{k}_F^\sigma = \frac{\hbar v_F k_F^\sigma}{\Delta_{so}}. \quad (\text{S.3})$$

Note that $\tilde{\Delta}_\pm = |\gamma \mp 1|/2$ and $\tilde{k}_F^\pm = \sqrt{\tilde{\mu}^2 - \tilde{\Delta}_\pm^2}$. In terms of $\tilde{\mu}$, $\tilde{\Delta}_\sigma$, \tilde{k}_F^σ , \tilde{q} and \tilde{r} , the screened potential is of the form

$$\phi(r) = \frac{Ze\Delta_{so}}{\kappa\hbar v_F} \psi(\tilde{r}), \quad (\text{S.4})$$

where

$$\psi(\tilde{r}) = \int_0^\infty \frac{J_0(\tilde{q}\tilde{r})}{\tilde{\varepsilon}(\tilde{q}, 0)} d\tilde{q}, \quad (\text{S.5})$$

and the static dielectric function can be expressed as,

$$\tilde{\varepsilon}(\tilde{q}, 0) = 1 + \frac{4\alpha_\kappa\tilde{\mu}}{\tilde{q}} \left[1 - \sum_{\sigma=\pm} \theta(\tilde{q} - 2\tilde{k}_F^\sigma) \left(\frac{\sqrt{\tilde{q}^2 - 4\tilde{k}_F^{\sigma 2}}}{4\tilde{q}} - \frac{\tilde{q}^2 - 4\tilde{\Delta}_\sigma^2}{8\tilde{q}\tilde{\mu}} \arctan \frac{\sqrt{\tilde{q}^2 - 4\tilde{k}_F^{\sigma 2}}}{2\tilde{\mu}} \right) \right]. \quad (\text{S.6})$$

It can be checked that (keep in mind $\tilde{k}_F^- \leq \tilde{k}_F^+$)

$$\tilde{\varepsilon}(\tilde{q} < 2\tilde{k}_F^-, 0) = 1 + 4\alpha_\kappa \tilde{\mu} / \tilde{q}, \quad (\text{S.7})$$

$$\tilde{\varepsilon}(\tilde{q} \rightarrow \infty, 0) = 1 + \alpha_\kappa \pi / 2. \quad (\text{S.8})$$

For convenience, we introduce two auxiliary functions which will be useful later. The first is

$$\bar{J}_0(z) \equiv z {}_1F_2\left(\frac{1}{2}; 1, \frac{3}{2}; -\frac{1}{4}z^2\right) - 1, \quad (\text{S.9})$$

which satisfies $\frac{d\bar{J}_0(z)}{dz} = J_0(z)$, where ${}_mF_n(\alpha_1, \dots, \alpha_m; \beta_1, \dots, \beta_n; z)$ is the generalized hypergeometric function [2]. For $z \gg 1$ the asymptotic expression reads [3],

$$\bar{J}_0(z) \approx \sqrt{\frac{2}{\pi z}} \sin\left(z - \frac{\pi}{4}\right). \quad (\text{S.10})$$

The second is

$$\hat{J}_0(z) = \frac{1}{2}z^2 {}_1F_2\left(\frac{1}{2}; \frac{3}{2}, 2; -\frac{1}{4}z^2\right) - z, \quad (\text{S.11})$$

which satisfies $\frac{d\hat{J}_0(z)}{dz} = \bar{J}_0(z)$. For $z \gg 1$ the asymptotic expression reads [3],

$$\hat{J}_0(z) \approx \sqrt{\frac{2}{\pi z}} \cos\left(z + \frac{3}{4}\pi\right). \quad (\text{S.12})$$

II. THE EVALUATION OF THE OSCILLATORY PART OF SCREENED POTENTIAL

In this section, we calculate the oscillatory part of the screened potential at large distance from a charged impurity ($\tilde{k}_F^- r \gg 1$). Integrating by parts leads to

$$\psi(\tilde{r}) = \frac{1}{\tilde{r}} \int_0^\infty \frac{d\bar{J}_0(\tilde{q}\tilde{r})}{\tilde{\varepsilon}(\tilde{q}, 0)} = \frac{1}{\tilde{r}} \left[\frac{\bar{J}_0(\tilde{q}\tilde{r})}{\tilde{\varepsilon}(\tilde{q}, 0)} \right]_0^\infty + \frac{1}{\tilde{r}} \int_0^\infty \frac{\bar{J}_0(\tilde{q}\tilde{r})}{\tilde{\varepsilon}(\tilde{q}, 0)^2} \frac{d\tilde{\varepsilon}(\tilde{q}, 0)}{d\tilde{q}} d\tilde{q}, \quad (\text{S.13})$$

From Eqs.(S.7), (S.8) and noticing that $\bar{J}_0(z \rightarrow 0) = -1$ and $\bar{J}_0(z \rightarrow \infty) = 0$ we find the underline term vanishes, then

$$\psi(\tilde{r}) = \frac{1}{\tilde{r}} \int_0^\infty \frac{\bar{J}_0(\tilde{q}\tilde{r})}{\tilde{\varepsilon}(\tilde{q}, 0)^2} \frac{d\tilde{\varepsilon}(\tilde{q}, 0)}{d\tilde{q}} d\tilde{q}. \quad (\text{S.14})$$

According to Lighthill theorem [5], the contribution of the integral comes only from the non-analyticity of the polarization function at $\tilde{q} = 2\tilde{k}_F^\pm$ where its derivatives are discontinuous. In this case, $\tilde{q} = 2\tilde{k}_F^-$ and $\tilde{q} = 2\tilde{k}_F^+$ are two singularities of the derivatives of the static polarization function (when $\gamma = 0$ the two singularities degenerate), therefore one can make the decomposition to pick up the main contribution

$$\psi(\tilde{r}) \approx \psi_{\tilde{k}_F^-}(\tilde{r}) + \psi_{\tilde{k}_F^+}(\tilde{r}). \quad (\text{S.14})$$

Around $\tilde{q} = 2\tilde{k}_F^\pm$ the static dielectric function reads

$$\tilde{\varepsilon}(\tilde{q} \approx 2\tilde{k}_F^\pm, 0) \approx 1 + \frac{2\alpha_\kappa \tilde{\mu}}{\tilde{k}_F^\pm} \tilde{f}_\pm, \quad (\text{S.15})$$

which is finite with

$$\tilde{f}_\pm = 1 - \frac{1 \pm 1}{2} \left(\frac{\sqrt{\tilde{k}_F^{+2} - \tilde{k}_F^{-2}}}{4\tilde{k}_F^+} - \frac{\tilde{k}_F^{+2} - \tilde{\Delta}^2}{4\tilde{k}_F^+ \tilde{\mu}} \arctan \frac{\sqrt{\tilde{k}_F^{+2} - \tilde{k}_F^{-2}}}{\tilde{\mu}} \right). \quad (\text{S.16})$$

A. For the case with $\gamma \neq 1$

For $\gamma \neq 1$ (namely, $\tilde{\Delta}_\pm \neq 0$), the first derivative of the static dielectric function $\frac{d\tilde{\varepsilon}(\tilde{q}, 0)}{d\tilde{q}}$ takes a form $\frac{\theta(\tilde{q} - 2\tilde{k}_F^\pm)}{\sqrt{\tilde{q} - 2\tilde{k}_F^\pm}}$ around $\tilde{q} = 2\tilde{k}_F^\pm$, and hence is divergent at $\tilde{q} = 2\tilde{k}_F^\pm$. In addition, the integrand $\frac{\tilde{J}_0(\tilde{q}\tilde{r})}{\tilde{\varepsilon}(\tilde{q}, 0)^2} \frac{d\tilde{\varepsilon}(\tilde{q}, 0)}{d\tilde{q}}$ in Eq.(S.14) and its first derivative behave well at both $\tilde{q} = 0$ and $\tilde{q} = \infty$. Therefore, according to Lighthill theorem,

$$\psi_{\tilde{k}_F^\pm}(\tilde{r}) \approx \frac{1}{\tilde{r}} \int_0^\infty \frac{\tilde{J}_0(\tilde{q}\tilde{r})}{\tilde{\varepsilon}(\tilde{q}, 0)^2} \frac{d\tilde{\varepsilon}(\tilde{q}, 0)}{d\tilde{q}} d\tilde{q} \Big|_{\tilde{q} \approx 2\tilde{k}_F^\pm}, \quad (\text{S.17})$$

with

$$\frac{d\tilde{\varepsilon}(\tilde{q}, 0)}{d\tilde{q}} \Big|_{\tilde{q} \approx 2\tilde{k}_F^\pm} \approx -\frac{\alpha_\kappa \tilde{\Delta}_\pm^2}{2\tilde{\mu} \tilde{k}_F^\pm \sqrt{\tilde{k}_F^\pm}} \frac{\theta(\tilde{q} - 2\tilde{k}_F^\pm)}{\sqrt{\tilde{q} - 2\tilde{k}_F^\pm}}. \quad (\text{S.18})$$

Substituting Eqs.(S.10), (S.15) and (S.18) into Eq.(S.17), and taking into account the integration

$$\int_0^\infty \frac{\sin(\tilde{q}\tilde{r} - \frac{\pi}{4}) \theta(\tilde{q} - 2\tilde{k}_F^\pm)}{\sqrt{\tilde{q} - 2\tilde{k}_F^\pm}} d\tilde{q} = \sqrt{\frac{\pi}{\tilde{r}}} \sin(2\tilde{k}_F^\pm \tilde{r}), \quad (\text{S.19})$$

we obtain the oscillatory part of the gapped case

$$\psi_{\tilde{k}_F^\pm}(\tilde{r}) \approx -\frac{\alpha_\kappa \tilde{\Delta}_\pm^2}{2\tilde{\mu}(\tilde{k}_F^\pm + 2\alpha_\kappa \tilde{\mu} \tilde{f}_\pm)^2} \frac{\sin(2\tilde{k}_F^\pm \tilde{r})}{\tilde{r}^2}. \quad (\text{S.20})$$

B. For the case with $\gamma = 1$

For $\gamma = 1$ (namely, $\tilde{\Delta}_- = 1$ and $\tilde{\Delta}_+ = 0$), at $\tilde{q} = 2\tilde{k}_F^-$ the first derivative of the static polarization function is divergent while at $\tilde{q} = 2\tilde{k}_F^+ = 2\tilde{\mu}$ the first derivative of the static polarization function is continuous but the second derivative is divergent. Consequently we are able to consider the first derivative around $\tilde{q} = 2\tilde{k}_F^-$ only but must take the second derivative around $\tilde{q} = 2\tilde{k}_F^+ = 2\tilde{\mu}$ into account.

For $\tilde{q} \approx 2\tilde{k}_F^-$, from Eq.(S.20) we have

$$\psi_{\tilde{k}_F^-}(\tilde{r}) \approx -\frac{\alpha_\kappa \tilde{\Delta}_-^2}{2\tilde{\mu}(\tilde{k}_F^- + 2\alpha_\kappa \tilde{\mu} \tilde{f}_-)^2} \frac{\sin(2\tilde{k}_F^- \tilde{r})}{\tilde{r}^2}. \quad (\text{S.21})$$

For $\tilde{q} \approx 2\tilde{k}_F^+$ we consider the second derivative

$$\begin{aligned} \psi_{\tilde{k}_F^+}(\tilde{r}) &\approx \frac{1}{\tilde{r}} \int_0^\infty \frac{\tilde{J}_0(\tilde{q}\tilde{r})}{\tilde{\varepsilon}(\tilde{q}, 0)^2} \frac{d\tilde{\varepsilon}(\tilde{q}, 0)}{d\tilde{q}} d\tilde{q} \Big|_{\tilde{q} \approx 2\tilde{k}_F^+} = \frac{1}{\tilde{r}^2} \int_0^\infty G(\tilde{q}) d\hat{J}_0(\tilde{q}\tilde{r}) \Big|_{\tilde{q} \approx 2\tilde{k}_F^+} \\ &= \left\{ \frac{1}{\tilde{r}^2} \left[G(\tilde{q}) \hat{J}_0(\tilde{q}\tilde{r}) \right]_0^\infty - \frac{1}{\tilde{r}^2} \int_0^\infty \hat{J}_0(\tilde{q}\tilde{r}) \frac{dG(\tilde{q})}{d\tilde{q}} d\tilde{q} \right\} \Big|_{\tilde{q} \approx 2\tilde{k}_F^+}, \end{aligned} \quad (\text{S.22})$$

where

$$G(\tilde{q}) = \frac{1}{\tilde{\varepsilon}(\tilde{q}, 0)^2} \frac{d\tilde{\varepsilon}(\tilde{q}, 0)}{d\tilde{q}}. \quad (\text{S.23})$$

It can be checked that the underlined term vanishes from $\hat{J}_0(z \rightarrow 0) = \hat{J}_0(z \rightarrow \infty) = 0$ and Eqs.(S.7), (S.8), then

$$\psi_{\tilde{k}_F^+}(\tilde{r}) = -\frac{1}{\tilde{r}^2} \int_0^\infty \hat{J}_0(\tilde{q}\tilde{r}) \frac{dG(\tilde{q})}{d\tilde{q}} d\tilde{q} \Big|_{\tilde{q} \approx 2\tilde{k}_F^+}. \quad (\text{S.24})$$

It is noted that the integrand $\hat{J}_0(\tilde{q}\tilde{r})\frac{dG(\tilde{q})}{d\tilde{q}}$ in Eq.(S.24) and its first derivative behave well at $\tilde{q} = 0$ and $\tilde{q} = \infty$. Because $\frac{d\tilde{\varepsilon}(\tilde{q},0)}{d\tilde{q}}\Big|_{\tilde{q}\approx 2\tilde{k}_F^+}$ is finite, we obtain

$$\frac{dG(\tilde{q})}{d\tilde{q}}\Big|_{\tilde{q}\approx 2\tilde{k}_F^+} \approx \frac{1}{\tilde{\varepsilon}(\tilde{q},0)^2} \frac{d^2\tilde{\varepsilon}(\tilde{q},0)}{d\tilde{q}^2}\Big|_{\tilde{q}\approx 2\tilde{k}_F^+}. \quad (\text{S.25})$$

with

$$\frac{d^2\tilde{\varepsilon}(\tilde{q},0)}{d\tilde{q}^2}\Big|_{\tilde{q}\approx 2\tilde{k}_F^+=2\tilde{\mu}} \approx \frac{\alpha_\kappa}{4\tilde{\mu}\sqrt{\tilde{\mu}}} \frac{\theta(\tilde{q}-2\tilde{\mu})}{\sqrt{\tilde{q}-2\tilde{\mu}}}. \quad (\text{S.26})$$

Therefore substituting Eqs.(S.12), (S.25) and (S.26) into Eq.(S.24), and using the integration

$$\int_0^\infty \frac{\cos(\tilde{q}\tilde{r} + \frac{3}{4}\pi)\theta(\tilde{q}-2\tilde{k}_F^+)}{\sqrt{\tilde{q}-2\tilde{k}_F^+}} d\tilde{q} = -\sqrt{\frac{\pi}{\tilde{r}}} \cos(2\tilde{k}_F^+\tilde{r}), \quad (\text{S.27})$$

we obtain that

$$\psi_{\tilde{k}_F^+}(\tilde{r}) \approx \frac{\alpha_\kappa}{4\tilde{\mu}^2(1+2\alpha_\kappa\tilde{f}_+)^2} \frac{\cos(2\tilde{k}_F^+\tilde{r})}{\tilde{r}^3}. \quad (\text{S.28})$$

III. SUMMARY

For $\gamma \neq 1$, the screened potential is

$$\phi_{\gamma \neq 1}(r) \approx \frac{Ze\Delta_{so}}{\kappa\hbar v_F} \sum_{\sigma=\pm} -\frac{\alpha_\kappa \tilde{\Delta}_\sigma^2}{2\tilde{\mu}(\tilde{k}_F^\sigma + 2\alpha_\kappa\tilde{\mu}\tilde{f}_\sigma)^2} \frac{\sin(2\tilde{k}_F^\sigma\tilde{r})}{\tilde{r}^2}. \quad (\text{S.29})$$

For $\gamma = 1$, $\tilde{\Delta}_- = 1$, $\tilde{\Delta}_+ = 0$ ($\tilde{k}_F^- = \sqrt{\tilde{\mu}^2 - 1}$, $\tilde{k}_F^+ = \tilde{\mu}$), the screened potential reads

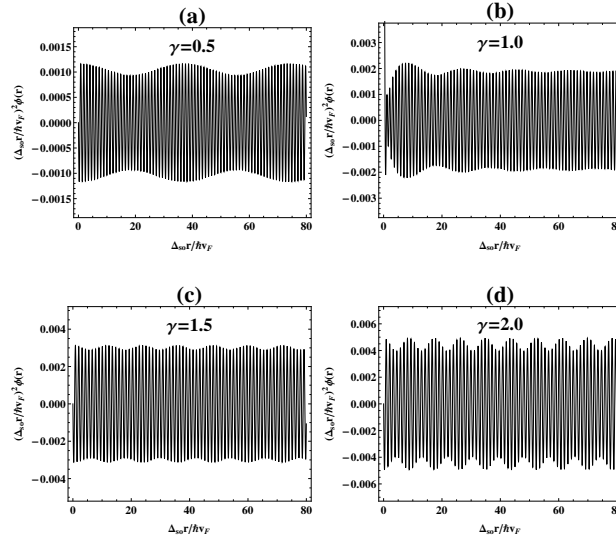


FIG. 5: The beating behavior of asymptotic screened potential (in units of $Ze\Delta_{so}/\kappa\hbar v_F$) versus the ratios γ by using the Lighthill theorem. We set $\kappa = 3$, $\mu = 3\Delta_{so}$ and $v_F = c/550$.

$$\phi_{\gamma=1}(r) = \frac{Ze\Delta_{so}}{\kappa\hbar v_F} \left(-\frac{\alpha_\kappa \tilde{\Delta}_-^2}{2\tilde{\mu}(\tilde{k}_F^- + 2\alpha_\kappa\tilde{\mu}\tilde{f}_-)^2} \frac{\sin(2\tilde{k}_F^-\tilde{r})}{\tilde{r}^2} + \frac{\alpha_\kappa}{4\tilde{\mu}^2(1+2\alpha_\kappa\tilde{f}_+)^2} \frac{\cos(2\tilde{\mu}\tilde{r})}{\tilde{r}^3} \right). \quad (\text{S.30})$$

In terms of μ , Δ_σ , k_F^σ and r , the screened potential reads

$$\phi_{\gamma \neq 1}(r) \approx \frac{Ze}{\kappa} [F_-(r) + F_+(r)], \quad (\text{S.31})$$

$$\phi_{\gamma=1}(r) \approx \frac{Ze}{\kappa} [F_-(r) + G_+(r)], \quad (\text{S.32})$$

where the functions $F_\pm(r)$, $G_+(r)$ and f_\pm are given by

$$F_\pm(r) = -\frac{\alpha_\kappa \hbar v_F \Delta_\pm^2}{2\mu(\hbar v_F k_F^\pm + 2\alpha_\kappa \mu f_\pm)^2} \frac{\sin(2k_F^\sigma r)}{r^2}, \quad (\text{S.33})$$

$$G_+(r) = \frac{\alpha_\kappa \hbar^2 v_F^2}{4\mu^2(1 + 2\alpha_\kappa f_+)^2} \frac{\cos(2k_F^+ r)}{r^3}, \quad (\text{S.34})$$

$$f_\pm = 1 - \frac{1 \pm 1}{2} \left(\frac{\sqrt{k_F^{+2} - k_F^{-2}}}{4k_F^+} - \frac{\hbar^2 v_F^2 k_F^{+2} - \Delta_-^2}{4\hbar v_F k_F^+ \mu} \arctan \frac{\hbar v_F \sqrt{k_F^{+2} - k_F^{-2}}}{\mu} \right). \quad (\text{S.35})$$

At last, we show that the analytical result in Eqs.(S.31) and (S.32)(see Fig. 5 in this supplementary material) is in good agreement with that in Fig. 3 in the main text in the large $\Delta_{so}r/\hbar v_F$ region.

-
- [1] W. A. Harrison, *Solid State Theory* (Dover Publications, New York, 1979).
 - [2] I. S. Gradshteyn and I. M. Ryzhik, *Table of Integrals, Series, and Products* (Academic Press, London, 2000).
 - [3] A. R. Miller and H. M. Srivastava, J. Austral. Math. Soc. Ser. B **40**, 222 (1998).
 - [4] M. Abramowitz and I. A. Stegun, *Handbook of Mathematical Functions: With Formulas, Graphs, and Mathematical Tables* (Dover Publications, New York, 1972).
 - [5] M. J. Lighthill, *Introduction to Fourier Analysis and Generalized Functions* (Cambridge University Press, Cambridge, 1958).